



Citation for published version:

Román, S, Ledesma, B, Álvarez, A & Herdes, C 2018, 'Towards sustainable micro-pollutants' removal from wastewaters: caffeine solubility, self-diffusion and adsorption studies from aqueous solutions into hydrochars', *Molecular Physics*, vol. 116, no. 15-16, pp. 2129-2141. <https://doi.org/10.1080/00268976.2018.1487597>

DOI:

[10.1080/00268976.2018.1487597](https://doi.org/10.1080/00268976.2018.1487597)

Publication date:

2018

Document Version

Peer reviewed version

[Link to publication](#)

This is an Accepted Manuscript of an article published by Taylor and Francis in *Molecular Physics* on 22 June 2018, available online: <https://www.tandfonline.com/doi/full/10.1080/00268976.2018.1487597>

University of Bath

Alternative formats

If you require this document in an alternative format, please contact:
openaccess@bath.ac.uk

General rights

Copyright and moral rights for the publications made accessible in the public portal are retained by the authors and/or other copyright owners and it is a condition of accessing publications that users recognise and abide by the legal requirements associated with these rights.

Take down policy

If you believe that this document breaches copyright please contact us providing details, and we will remove access to the work immediately and investigate your claim.

Towards sustainable micro-pollutants removal from wastewaters: Caffeine solubility, self-diffusion and adsorption studies from aqueous solutions into hydrochars

S. Román⁽¹⁾, B. Ledesma⁽¹⁾, A. Álvarez⁽¹⁾ and C. Herdes^{(2)*}

⁽¹⁾ *Departamento de Física Aplicada, Universidad de Extremadura, Avda. Elvas s/n 06071, Spain.*

⁽²⁾ *Department of Chemical Engineering, University of Bath, Claverton Down, Bath, Somerset BA2 7AY, United Kingdom.*

*Corresponding author e-mail: c.e.herdes.moreno@bath.ac.uk

Keywords: hydrocarbonization, adsorption, molecular dynamics, mean square displacement, BAR method.

ABSTRACT

Hydrochars obtained via hydrothermal carbonization of pistachio shells are both a sustainable and an efficient alternative to commercial activated carbons for the removal of micro-pollutants from wastewaters that are difficult to handle by conventional treatments. Here a combined experimental and molecular simulation approach is adopted for the study of the caffeine/hydrochars aqueous systems. This case study serves to tune a general framework for the rational customization of surface functional groups on hydrochars for the selective adsorption of micro-pollutants from wastewaters. Caffeine's solubility, self-diffusion and adsorption results from aqueous solutions at relevant conditions are presented. Insights about the role of surface functional groups over the caffeine adsorption mechanism into hydrochars are gained and discussed.

1. INTRODUCTION

Nowadays, the number of micro-pollutants that are difficult to handle by conventional treatments are both ubiquitous and on the rise in wastewaters. These unprocessed contaminants are having a worldwide negative impact, due to their persisting accumulation in aquatic environments. Micro-pollutants' sources range from complex industrial processes to our most mundane activities such as taking a shower or washing our clothes (with non-biodegradable surfactants), taking our medicines (rather pharmacological drugs been incompletely metabolized and secreted by our bodies) and even making and drinking our coffees.

Caffeine (CAF) is one of the most popular drugs. Since CAF can be (almost entirely) attributed to human use it is usually proposed as a tracer of anthropogenic contamination. CAF has been found in well-water [1], seawater [2], lakes and rivers [3] and is generally present in sewage and surface water effluents, having been detected in the latest at maximum levels of 6.0 mg L⁻¹ [4].

Adsorption has been used as an effective alternative in the elimination of micro-pollutants from wastewater [5-7]. Commercial adsorbents, such as activated carbons (ACs), which generally show a micro-porous character, have been tested for the removal of these compounds, resulting in extended times of operation, suggesting a

diffusion controlled system. Alternatively, mesoporous coals may adsorb larger molecules, such as dyes or organic compounds, providing better dynamic performance.

Despite the well-proven performance of ACs, their increasing demand calls for the search of new precursors as well as novel and more sustainable manufacturing methodologies. In this frame, hydrothermal carbonization (HTC) outstands because of its low cost, simplicity and possibility to broaden the use of raw materials, as compared to traditional activation processes.

Recently, scientists all over the world have tried to demonstrate that HTC is an effective way to convert biomass into carbonaceous materials and to understand how to drive the process in order to maximize the solid yield, carbon or nitrogen capture and surface properties [8-10]. The appropriate design of surface properties (both pore structure and chemical functionalities) is essential to provide good adsorption results towards a given adsorbate and have been the topic of research for many years in the AC field. However, with the current push on HTC processes seeking for particular features especially in regard to the potential to tune up the nature and quantity of the final adsorbent's surface functional groups, which in turn can improve adsorption selectivity [11], the efforts on the search of manufacturing methods have increased exponentially.

HTC has the significant advantage over classical pyrolysis (a needed preceding step for physical activation) of keeping most of the oxygen surface functional groups, thus yielding an overall acidic surface on the HC – whereas chars obtained by pyrolysis lose their oxygen functionalities and have a predominance of basic groups [8]. Moreover, recent works point out that pyrolysed HCs (i.e. after their thermal treatment) could either keep their newly created surface functionalities or these would be modified according to defined mechanisms [12] both alternatives due to the fact of subjecting the biomass to HTC prior to charring. The HTC capability to provide additional ways to control the creation of specific groups on the HC surface is a formidable gain and can be seen as a tool to understand adsorption mechanisms and improve the performance of adsorbents.

A few recent pieces of research have been devoted to the study of HCs or HC derived materials for the adsorption of pharmaceuticals and personal care products [13]. Fernandez et al. studied the effect of HC from orange peels as adsorbents for diclofenac sodium, salicylic acid and flurbiprofen. The HC's capacity to adsorb the three contaminants was found largely dependent on whether the molecules were ionized or in their neutral form and on the porosity of the adsorbents [11]. Kirschhöfer et al. successfully adsorbed sulfamethoxazole, carbamazepine, bezafibrate and diclofenac in HC from sewage sludge [14].

In the particular case of CAF adsorption processes, our aqueous CAF adsorption studies [8-9] pointed out the need of diffusion and free energy calculations (or residual chemical potential) at different temperatures to be performed, in order to establish the dynamic and energetic landscape of CAF on the HC surfaces and on the aqueous phase, to estimate the driving forces and energetic cost (diffusion and free energy difference) between absorbed and bulk phases, key information for the rational customization of HCs for CAF removal. It is worth noticing that our approach can be easily tailored for the sequestration of any other micro-pollutants.

Currently, the estimation of self-diffusion coefficients and free energies using molecular simulation techniques has attracted much interest in areas such as drug design and material science – it is worth noticing that this work solely refers to the diffusion of caffeine as its self-diffusion coefficient. Given an appropriate description of the molecular interactions (i.e. the Hamiltonian), the diffusion of selected species can be calculated from molecular dynamics (MD) simulations by tracking the mean square displacement of such compounds as a function of time, without the limiting constraint of infinite dilution of experimental systems. Common free energy types include the solvation, transfer, binding and conformational free energy. The ability to calculate accurate estimates of the free energy from molecular simulations overcomes the difficult experimental measurement of these relevant thermodynamic properties of a system. Conversely, to obtain a reliable estimate of the free energy of a system from molecular simulations, some challenges must be met [15-16]. The most common methods to estimate free energy are thermodynamic integration, free energy perturbation, umbrella sampling and potential of mean force [15-16].

In this contribution, different HCs for CAF adsorption were produced and evaluated on our wet laboratory, to assess the effect of the chemical and textural surface in the adsorption of this drug, alongside molecular modelling framework for the CAF self-diffusion and free energy calculations is presented and validated, the discussion of case studies in bulk and two HC pore width at relevant conditions is also given.

2. EXPERIMENTAL STUDIES

2.1. Materials

Pistachio shells from Extremadura (southwest Spain), were provided by local suppliers, washed and oven-dried at 100 °C. The dried samples were then crushed, milled and screen-sieved (0.5–1 mm). The precursor material obtained is hereafter abbreviated as PS. The proximate analysis of the precursor, assessed by means of an automatic elemental analyser (Carlo Erba model EA 1108) indicated a carbon content of 46.5%, close to the proportion of other similar biomass resources previously used by us for HTC processes such as walnut shell or olive stone [17]. Oxygen and hydrogen were, respectively, 47.11 and 6.39% while S and N were not detected and this is an advantage regarding the subsequent use of the precursor during thermochemical processes, due to the minimization of hazardous compounds. Pure caffeine (Sigma-Aldrich S.L.) was used as the adsorbate.

2.2. Production of HCs

A mass of 10 g of PS was soaked with 100 g of distilled water and allowed to hydrate for 2 h within a Teflon vessel. HTC processes were carried out in a stainless-steel autoclave (Berghof, Germany), heated at 220 °C for 20 h under self-generated pressure conditions. These experimental conditions were chosen based on previous works with agricultural residues [17]. Then, the sample was rapidly cooled to room temperature immersing the reactor in an ice bath, and the solid was collected by filtration and sequentially washed with warm distilled water and finally dried at 100 °C.

The modification of the reaction pathways and in consequence the incorporation of new

functionalities on the HC surface was investigated by adding chemicals to the reaction autoclave. The acidic reaction environment was set by adding HNO₃ (0.1 M) to the autoclave, while KOH (0.1 M) was used to increase the solution pH. In the first case, 1 g of the acid solution was used, while 0.1 g were used in the case of KOH. These samples were named, respectively, HC_Ac and HC_Ba.

Further pyrolysis of the HCs was also investigated, as it has been reported to favour the development of the surface area as a consequence of the removal of condensable blocking porosity and the removal of products from the previous chemical activation reactions. Pyrolysis was made in a vertical tubular stainless steel reactor described elsewhere [11] at 600 °C during 1 h, using N₂ (100 mL min⁻¹) as the inert gas. These samples were named, HC_Pir, HC_Ac_Pir and HC_Ba_Pir. Figure 1 provides a schematic representation of the different activation procedures employed, along with the acronyms used for the resulting products.

2.3. Characterization of HCs

2.3.1. Textural characterization

Textural properties were assessed by N₂ adsorption isotherms at 77 K (AUTOSORB-1, Quantachrome), according to conventional procedures. The Brunauer–Emmett–Teller (BET) surface area (S_{BET}) was determined by the standard BET procedure; total pore volume (V_t) was estimated from the amount of nitrogen adsorbed at the relative pressure of 0.95, and the mean pore width (W) was calculated from $W = 4 V_t / S_{\text{BET}}$. The external surface (S_{ext}) was assessed by the *a-method*, using a reference non-porous solid, as described in previous works [8], the volume of micropores was determined through the Dubinin–Radushkevich equation (V_{miDR}), and the volume of mesopores (V_{me}) was estimated as the difference between V_t and V_{miDR} .

Scanning electron microscopy (SEM) was performed in a Zeiss Supra 40 microscope equipped with a field emission gun. The images were taken with an in-lens detector and acceleration voltage was set at 3 kV. The samples were placed on an aluminium holder, supported on conductive carbon tape and sputter coated with Pt.

2.3.2. Chemical characterization

Elemental composition of the samples was assessed by means of an automatic elemental analyzer (Carlo Erba model EA 1108). Their surface chemistry was studied through the determination of the point of zero charge (PZC). It was estimated from the pH of a concentrated dispersion, following the procedure given in detail elsewhere [18]. Identification of surface functionalities was complementarily conducted by Fourier Transformed infrared (FT-IR) spectroscopy. The spectra were recorded by transmission method (Perkin-Elmer IR Spectrum BXII spectrometer) within the wavenumber range 600–4000 cm⁻¹.

2.4. Batch adsorption studies

CAF batch adsorption experiments were performed in glass flasks within a batch thermostated system (P SELECTA, Unitronic), at 25 ± 1 °C, under a wrist-action shaker agitation at 500 rpm. Adsorption tests were performed contacting 0.01 g of HC

with 15 mL of CAF solutions of different initial concentrations ($0.02\text{--}1\text{ g L}^{-1}$) during 48 h. Previous kinetic studies showed that this time was enough to assure equilibrium adsorbent-adsorbate. The concentrations of CAF in solution were obtained from the measured absorbance in the supernatant at their k_{max} (nm, respectively) by means of a UV-Vis spectrophotometer (Shimadzu Model UV mini 1240). Tests were carried out at least in duplicate. Average values are reported.

Adsorption equilibrium data were fitted to Freundlich and Langmuir models; both provide information on aspects such as adsorption affinity and capacity. However, since the affinity of the adsorbents towards the CAF was in some cases very low, and in consequence, very bad adjustments were found, this study only reports on the parameters obtained for those samples showing a good fitting (that is, L-type isotherms), as it is described in section 3.2.

3. SIMULATION STUDIES

3.1. Hamiltonian selection and validation by self-diffusion calculation

Suitable molecular models for the CAF and water system were evaluated [19]. An MD approach was employed to determine the influence of CAF concentration over self-diffusion in aqueous systems. For the sake of generality of the presented framework, the OPLS-AA force field [20] was selected for the description of micro-pollutants, in this specific case study the CAF molecules - advantages and limitations of this force field for the prediction of thermophysical properties have been comprehensively reviewed elsewhere [21]- meanwhile the water molecules followed four different parameterisations, specifically SPC, SPCE, TIP3P and TIP4P [22-25]. As in our previous work [26], the hydrochars' pore walls in a unit cell were mimicked by an array of carbon-atom layers with a surface area of $10 \times 10\text{ nm}^2$; each pore wall is composed of three stacked graphite layers with an interlayer spacing of 0.335 nm, described by the Steele's carbon potential [27]. The common Lorentz-Berthelot mixing rules were applied to calculate the interaction of heteroatomic pairs.

The MD trajectories, under representative ensembles (NVT, NPT, NPzzAT), were integrated using GROMACS [28]. The mean square displacements of CAF molecules in water were used to calculate the self-diffusion coefficient by the GROMACS post-processing function `g_msd` [28] applied over equilibrated simulations under the NVT ensemble (where the number of molecules, volume and temperature are kept constant). The NPzzAT was employed to mimic the CAF batch adsorption studies. In an NPzzAT cell, the number of molecules is fixed, the pressure coupling is isotropic in the x and y directions (i.e. P_{xx} and P_{yy} component of the pressure tensor are equal), but variable in the z -direction (i.e. P_{zz} is allowed to oscillate around a set point), the xy -area, perpendicular to the P_{zz} , and the temperature are also kept constant. We have tested the versatility of this ensemble in vapour-liquid equilibria and adsorption studies [29-30]. The NPT ensemble was used for the calculation of water densities at needed state points, as sanity checks of the water models implementation, and for the global equilibration in the Bennett acceptance ratio (BAR) method [31]. The Berendsen thermostat and barostat were selected as the coupling algorithms for all simulations. The

comparison between the calculated self-diffusion and available experimental value serve as validation of the models, this is discussed in detail in the results section.

3.2. Free energy of solvation via BAR method

The BAR method [31] was chosen for the estimation of CAF free energy in the studied systems. The BAR method agrees very well when compared to the free energy perturbation and the thermodynamic integration methods [32]. Advantageously, the BAR method has been implemented in GROMACS 5.x versions and online hands-on tutorials already exist to guide its application for small molecules such methane and ethanol in water.

$$E_{\text{Total}} = \lambda*(E_{\text{M-M}} + E_{\text{M-S}}) + E_{\text{S-S}} \quad (\text{Eq. 1})$$

In a nutshell, for the estimation of the free energy of solvation, the BAR method relies on consecutive simulations in which their total energy (E_{Total}) just differs in the “intensity” (λ) of a solute molecule (M) in solution (S), as described in equation 1 and depicted in Figure 2.

4. RESULTS & DISCUSSION

4.1. Surface analyses of HCs

N₂ adsorption at 77 K was the first analysis used to study the porous structure of the HCs obtained by the procedures described in section 2.2. Figure 3 depicts the adsorption isotherms for both non-pyrolysed and pyrolysed HCs. From the adsorption isotherms, characteristic textural parameters were determined according to the models described in section 2.3. Bestowing to their shape, the isotherms of the HCs (Figure 3) can be classified as type II (B.D.D.T. [33]), indicative of meso or macroporous solids with scarce microporosity. In these solids, the N₂ uptake at low values of relative pressure was negligible and the adsorbate volume increased gradually for higher values of relative pressure. Dissimilarly, the isotherms of samples subjected to pyrolysis after HTC exhibit a remarkable amount of N₂ adsorption at low values of P/P₀, suggesting a type-I shape and thus a developed microporosity on these materials, which in addition contain a significant volume of wider pores, since the plateau does exhibit a slight slope within the whole P/P₀ range, and there is also a significant N₂ uptake at P/P₀ values close to 1.

These results are in agreement with previous studies on HTC of biomass precursors; firstly, the process alone does not remove the condensable products from the porous matrix; although a small increase in N₂ adsorption is found for acid and base treated HCs, the prevalence of products from the chemical reactions involved does not improve the blockage of the porosity. The scarce porosity of HCs has been extensively reported [11, 17].

The HC subsequent pyrolysis brings up a clear development of the HC’s microporosity in all cases. The thermal treatment can help the removal of condensation products blocking porosity and part of the surface functionalities of the HCs. Despite the microporous character of all pyrolysed HCs, they also exhibit a clear contribution of wider pores, as deduced from the growing volume, at high P/P₀ values. Also, under the

experimental conditions used, while the use of acid involves a slight increase on the apparent surface of the HC, the treatment with KOH does improve the porosity development, as long as pyrolysis is used.

Table 1. Textural properties of HCs as determined from N₂ adsorption data and point of zero charge.

	$S_{\text{BET}}, \text{m}^2\text{g}^{-1}$	$V_{\text{mi(DR)}}, \text{cm}^3\text{g}^{-1}$	$V_{\text{me}}, \text{cm}^3\text{g}^{-1}$	$S_{\text{EXT}}, \text{m}^2\text{g}^{-1}$	$S_{\text{INT}}, \%$	PZC -
HC	15	0.008	0.019	22	0	4.18
HC_Ac	20	0.011	0.023	26	0	3.87
HC_Ba	16	0.008	0.014	17	0	6.42
HC_Pir	364	0.191	0.042	59	81	10.48
HC_Pir_Ac	387	0.203	0.099	73	77	4.57
HC_Pir_Ba	240	0.130	0.036	89	55	7.89

The surface morphology of the HCs was explored by SEM. Figures 4 to 6 show SEM of HCs and pyrolysed HCs, without chemical treatment (Figure 4), with basic treatment (Figure 5) and with acid treatment (Figure 6).

In all cases, the presence of microspheres can be highlighted. These features, usually reported for biomass-based HCs, can be associated to the reorganization of hemicellulose and cellulose fragments, into higher molecular weight compounds by polymerization and condensation reactions [34]. It is worth mentioning that these microspheres, very abundant for the sample obtained by simple HTC (HC) do not disappear after pyrolysis (HC_Pir, see Figure 4) but are mostly removed as a consequence of the post-treatment if KOH or HNO₃ are used during HTC. The prevalence of microspheres after pyrolysis suggests that lignin might also be one of their constituents.

The acid or base treatment during HTC has a clear effect on the HC morphology. The SEM of HC_Ba (Figure 5) shows a remarkable appearance of cavities and fragments resultant from the material degradation, together with the decrease on microspheres. In the case of HC_Ac (Figure 6) there is an abundance of microspheres with a lower diameter as compared to HC. Then, both materials (HC_Ba and HC_Ac) undergo a remarkable change after pyrolysis; the removal of products from the chemical reactions between acid/base and the biomass gives rise in both cases to an important decrease in the mass density and render clearly visible the cellular matrix of the precursor.

Although HCs are assumed to be acid materials, as a consequence of the acid environment created during HTC reactions, the modification of their surface functionalities is regarded as a powerful tool, because of the significant role of these features on subsequent HCs applications. The analysis of the point of zero charge of the materials (included in Table 1) provides a quick and effective technique to assess the predominance of acid or basic surface compounds. From the values shown in Table 1, it is evident that the original acidity of the HC becomes milder as a consequence of pyrolysis, due to the removal of oxygen functionalities due to the thermal treatment. The addition of KOH or HNO₃ brings out a slight decrease of the PZC and also makes the carbon surface less vulnerable to change upon heating, as the subsequent increase of

PZC as a result of heating is lower, as compared to HC_Pir, especially for the HC_Ac_Pir. This, in turn, confirms the potential of HTC as pre-treatment to develop stable surface chemistry target materials [12].

The FT-IR spectra of the HCs studied (Figure 7) also confirm these important differences; the band assignment was made according to suitable bibliography [35]. Several remarks can be made from the analyses of the spectra. Probably, the most prominent one, at a first glance, is the clear loss of HC oxygen functionalities as a consequence of pyrolysis, which is definitely milder in the case of KOH treatment; that is to say, the surface functionalities created in the HC surface as a consequence KOH chemical activation are significantly resistant to heating at 600°C.

In general, in all samples, several common bands can be identified, such as:

- Wideband 3400 cm^{-1} that can be attributed to O–H stretching vibrations which confirm the presence of oxygen in HC in the form of OH, which is usually attributed to the presence of humidity in the samples. The band at $1050\text{--}1100\text{ cm}^{-1}$ is also consistent with the existence of secondary OH groups.
- The signal at around 2400 cm^{-1} that can be related to C=O bonds in functional groups such as ketones.
- Bands centred at around 2900 cm^{-1} and 475 cm^{-1} that can be assigned to aliphatic C-H stretching vibrations and aromatic C-H bending vibrations confirming the existence of aliphatic compounds and aromatic compounds; bands at 1700 cm^{-1} and 1600 cm^{-1} which can be assigned to the C=O asymmetric stretching in carboxyl group and C=C vibrations, respectively. Both bands suggest the decarboxylation reaction and the aromatization of the biomass during hydrothermal treatment.
- Bands centred at 1600 cm^{-1} and 1475 cm^{-1} indicated aromatic stretching C=C vibrations
- The signal around 830 cm^{-1} is characteristic of p-substituted phenyl groups.

Among the changes induced on the surface chemistry on chemically treated HCs the following ones can be highlighted:

- Marked band centred at 1700 cm^{-1} in samples not subjected to pyrolysis (with the exception of HC_Ba_Pir), suggesting the presence of C=O in carboxyl in carboxyl groups.
- Intense band at around 1250 cm^{-1} , indicative of C-O vibrations in carboxyl groups and ether structures (again, this band is hard to distinguish after pyrolysis, excluding the sample treated with KOH, suggesting a lower thermolability of the groups).
- Well-defined bands at 1000 and 1100 cm^{-1} in HC_Ba and HC_Ba_Pir. These bands are soft (HC) or inexistent in the case of the other samples.

- Band near 1375 cm^{-1} , typical of methyl groups, which becomes more important for chemically treated HCs, and once more, disappears after pyrolysis for HC_Pir and HC_Ac_Pir, but not for HC_Ba_Pir.

These results are indicative of a modification of HCs after pyrolysis (less evident for basic materials) in which a greater presence of aromatic bonds is found. Previous reports on HTC of glucose have shown that during pyrolysis of HCs, $\text{sp}^3\text{ C-X}$ (X: e.g., C, O, H) bonds are transformed into aromatic $\text{sp}^2\text{ C=C}$ bonds to form a dense graphitic structure [36].

3.2. CAF adsorption isotherms

The adsorption performance of all the HCs was tested using CAF as adsorbate, following the procedure described in section 2.4. The results showed that although textural properties played an important role in the process, surface chemistry analyses confirmed that the existence and amount of specific surface groups were more important.

The adsorption of organic molecules is a very complex process, influenced by many factors such as the properties of the solvent (pH, molecule properties, etc.) and adsorbate (solubility, pKa and ionization, molecular size, type of substituent, etc.) as well as the adsorbent type (apparent surface, type of porosity, surface chemistry, etc.).

CAF experimental adsorption isotherms are displayed in Figure 8. Both Langmuir and Freundlich models were applied to all samples, however, just the experimental adsorption data of samples HC_Ac, HC_Ac_Pir, HC_Pir and HC_Ba_Pir showed a good adjustment, the characteristic parameters obtained for them was reported in Table 2. In Figure 8, only the theoretical data corresponding to fitting to Langmuir model has been shown, since it provided better results than the Freundlich one.

Table 2. Characteristic adsorption parameters as determined from application of Langmuir and Freundlich models to CAF adsorption data of selected HCs.

Langmuir		q_{\max} , mg g^{-1}	b , L g^{-1}	R^2
	HC_Pir	5.51	0.642	0.993
	HC_Ac	22.60	0.040	0.993
	HC_Ac_Pir	12.95	1.032	0.993
	HC_Ba_Pir	6.04	0.037	0.679
Freundlich		n_F	k_F , $\text{mg g}^{-1}(\text{mg L}^{-1})^{-n}$	R^2
	HC_Pir	-	-	-
	HC_Ac	0.97	0.30	0.971
	HC_Ac_Pir	1.39	2.89	0.959
	HC_Ba_Pir	3.17	1.04	0.721

The experimental results showed that acidic adsorbents had a better performance (HC_Ac and HC_Ac_Pir). Focussing on these two samples, it is very interesting to notice that i) the sample HC_Ac provided the best adsorption results despite its very low apparent surface, as deduced from the q_{\max} values (see Table 2) and, ii) that there is a significant difference on the isotherm slope of these two samples, indicative of very strong differences in adsorption affinity towards CAF. This information can also be deduced from the value of parameter b (Langmuir model), indicative of adsorption energy.

Above results, in turn, suggest that the development of microporosity brought up by pyrolysis can enhance adsorption at low values of C_{eq} , although the removal of surface oxygen functionalities from the adsorbent is seen as a drawback because it involves a lower participation of specific interactions adsorbate-adsorbent, decreasing the adsorption of CAF for high values of C_{eq} . In other words, the joint effect of a lower pore size (see Table 1; 77% of the porosity of HC_Ac_Pir is considered as internal porosity, i.e., microporosity, in relation to 0% for HC_Ac) and less acidic surface (3.8 vs. 4.6) makes the pyrolysis post-treatment inefficient if high concentrations of CAF are to be used.

Furthermore, the results also show that the use of KOH does not involve any remarkable advantage on CAF adsorption. In contrast to HNO_3 treated adsorbents, the surface functionalities developed in the former case bring out a decrease on adsorption energy, probably because of specific repulsive interactions or because of steric hindrance effects, which are not significantly improved after pyrolysis. Indeed, the results found for the HC_Ba were the worst and the further pyrolysis of this sample improved the results very little, despite the great increase in S_{BET} , probably because the strong resistance of KOH induced surface groups upon heating (see Figure 7).

Understanding of the causes of these results is a very complex task since several factors have to be considered. For example, dispersive π - π interactions (which might be at first expected due to the aromatic ring in CAF molecule) do not seem to play a predominant

role in the adsorption mechanisms. As previously reported [37], acidic surface groups tend to localize the surface π -electrons of ACs, decreasing their availability, which would correspond to worse adsorption results for HC_Ac and HC_Ac_Pir. The prominence of non-dispersive interactions (such as specific interactions between CAF nitro group and oxygen groups) might be therefore more important.

Other plausible effects might be related to i) the fact that water molecules compete with CAF ones, ii) differences in caffeine solubility or iii) changes on the self-diffusion in water systems, as a consequence of the change in pH for each run.

Further insights on the effect of the surface chemistry on CAF adsorption were obtained by simulation studies tracking the behaviour of CAF molecules in combining bulk and pore zones, as can be seen in Figure 9.

3.3. CAF self-diffusion

MD was employed here to calculate the CAF self-diffusion coefficients in the water bulk and into two HC pores, specifically 2 nm and 5 nm widths, with (PA) and without (PN) acid groups (hydroxyl, OH), and as a function of bulk CAF concentrations.

3.3.1 Influence of CAF concentration over self-diffusion in aqueous systems.

The experimental measurement of self-diffusion coefficients presents a challenge for a stepwise associating solute as CAF, where a 0.1 mol L^{-1} (19 g L^{-1}) CAF solution at 298K will have just 40% of CAF monomers, 30% of CAF dimmers and the remainder will exist as higher size aggregates [38].

CAF aqueous concentrations for viable atomistic simulations are one to three orders of magnitude higher than the experimental ones for diffusion or adsorption studies, respectively. However, in the simulation realm, it is easy to set a single CAF monomer diffusion study, at an apparent high bulk concentration (16 g L^{-1}), these results are summarised in Figure 10.

CAF/SPCE presented the overall best performance for the calculation of bulk CAF self-diffusion coefficient in aqueous systems, 0.7412×10^{-9} ($\pm 0.0313 \times 10^{-9}$) $\text{m}^2 \text{ s}^{-1}$ as compared with available experimental data ($0.7731 \times 10^{-9} \text{ m}^2 \text{ s}^{-1}$) [39]. Therefore this pair of molecular models was selected for further simulations.

3.3.2. Influence of HC synthesis conditions over its aqueous CAF uptake.

A molecular simulation cell, of 22 g L^{-1} initial CAF concentration, was presented to a water-saturated HC structure of 2 nm and 5 nm (with and without surface OH groups) until the whole system attained equilibrium. Results for 2 nm HC PN are shown in Figures 11a and 11b for the evolution of particular pair energies and selected MD snapshots, respectively.

The equilibrated system presents the CAF-HC adsorption energy as the most favourable one, followed by the CAF-Water and CAF-CAF interactions. However, the adsorption energy trade from a 2 nm HC PN seems not able to promote the disaggregation of CAF clusters in the aqueous bulk. The 2 nm HC PN presents a stepwise uptake, due to the formation of dimmers, and higher size aggregates, that quickly ($< 2 \text{ ns}$) block the pore entrance. It is also worth noticing that not rearrangement of these “blocking aggregates”

was attained even after 4 ns. The 5 nm HC PN presents similar CAF bulk/pore distribution, however, a central bulk-like zone was developed in equilibrium with the adsorbed phase. A distinctive behaviour was found with HCs PA (analogous initial simulation cell but with 3% mol OH groups randomly distributed on the pore inner surface) where OH surface groups allowed higher uptake of CAF by promoting a monolayer formation, preventing a premature pore blockage due to CAF self-aggregation.

3.4. CAF free energy of solvation

A lengthy process is needed to set the simulations before employing the BAR method for its analysis, however, GROMACS makes its application a straightforward task. The needed steps, previous to the extraction of the energy of solvation (ΔG) via BAR, are described in the flow diagram shown in Figure 12a.

Following the above procedure (Figure 12a), Figure 12b shows the contribution to the CAF ΔG of solvation from consecutive 21 λ -points. Convergence between adjacent λ -points was established by evaluating their entropic difference [40]. The total CAF ΔG of solvation at 298K was estimated in $-56.81(\pm 0.39)$ kJ mol⁻¹, in good agreement with the experimental value of $-52.89(\pm 3.10)$ kJ mol⁻¹ [41].

5. CONCLUSIONS

Hydrothermal carbonization (HTC) of pistachio nutshell is an effective and low-cost method to produce low-porosity carbon materials with a wide variety of functionalities, predominantly acidic in nature. The addition of acid (HNO₃) or base (KOH) does not improve the pore volume, although it does alter the surface appearance of the materials and especially involves an important modification of their surface chemistry.

Furthermore, pyrolyzing these materials brings out a very important improvement on the porous structure of the HCs, rendering a more micro-porous structure, as a result of the removal of products blocking porosity. This post-treatment also brings out the disappearance of several thermolabile oxygen functionalities, with a net increase of surface acidity; this effect was remarkably less important for the HC prepared with KOH (HC_Ba).

Caffeine adsorption was studied both experimentally and by molecular simulation. Based on the results of our combined methodology an adsorption mechanism can be elucidated to remove CAF using micro-porous HCs. Previous to CAF intake in HC, the CAF aggregates in the bulk could be dissolved by the presence of active acid groups (OH) in the external surface of the HCs disrupting the CAF π - π aromatic interactions, additional OH groups in the internal surface of the pores could also prevent pore blockage promoting the formation of a CAF monolayer.

The presented Hamiltonian, diffusion and free energy estimation methods are currently being used to further study the CAF/Water/HC systems at different conditions, to find the optimal HC surface modification for the selective adsorption of CAF. Moreover, the combined experimental/molecular simulation methodology adopted here can be tuned for the study of the adsorption behaviour of other micro-pollutants in HCs from aqueous systems.

6. ACKNOWLEDGEMENTS

This work has received funding from “Junta de Extremadura“ through project IB16108, and from “Ministerio de Economía y Competitividad”, via project CTM2016-75937-R. Also, the authors thank the Service “SAIUEX” (Servicios de Apoyo a la Investigación de la Universidad de Extremadura) for Surface characterization analyses. CH acknowledges the use of Balena, the HPC cluster at the University of Bath for the presented MD calculations.

References

- [1] R. L. Seiler, S. D. Zaugg, J. M. Thomas, D. L. Howcroft, *Ground Water* **37**, 405 (1999).
- [2] R. Siegener and R. F. Chen, *Mar. Pollut. Bull.* **44**, 383 (2002).
- [3] I. J. Buerge, T. Poiger, M. D. Müller, H. R. Buser, *Environ. Sci. Technol.* **37**, 691 (2003).
- [4] D. W. Kolpin, M. Skopec, M. T. Meyer, E. T. Furlong, S. D. Zaugg, *Sci. Total Environ.* **328**, 119 (2004).
- [5] P.C.C. Faria, J.J.M. Órfao, J.L. Figueiredo, M.F.R. Pereira, *Appl. Surf. Sci.* **254**, 3497 (2008).
- [6] J. L. Sotelo, G. Ovejero, A. Rodríguez, S. Álvarez, J. García, *Sep. Sci. Tech.* **48**, 2626 (2013).
- [7] J. L. Sotelo, G. Ovejero, A. Rodríguez, S. Álvarez, J. García, *Chem. Eng. J.* **228**, 102 (2013).
- [8] S. Román, J.M. Nabais, B. Ledesma, J.F. González, C. Laginhas, M.M. Titirici. *Micropor. Mesopor. Mat.* **165**, 127 (2013).
- [9] T. Reza, S. Román, S. Poulson, C.J. Coronella. *J Anal Appl Pyrol*, in press (2018)
- [10] U. Ekpo, A. B. Ross, M.A. Camargo-Valero, P.T. Williams. *Biores. Technol.* **200**, 951 (2016).
- [11] M. E. Fernández, B. Ledesma, S. Román, P.R. Bonelli, A. L. Cukierman. *Biores. Technol.* **183**, 221 (2015).
- [12] A. Jain, R. Balasubramanian, M.P. Srinivasan. *Chem. Eng. J.* **283**, 789 (2016).
- [13] Shirts, et al. *J Chem Phys* **119**, 5740 (2003).
- [14] Román, et al. *Energies* **11**, 216 (2018).
- [15] Kirschhöfer, et al. *Water Sci. Technol.* **73**(3), 607 (2016).
- [16] Christ, et al. *J Comput Chem* **31**, 1569 (2010).
- [17] S. Román, J. Nabais, B. Ledesma, C. Laginhas. *Fuel Process Tech.* **103**, 78 (2012).
- [18] P.J.M., Carrott, J.M.V. Nabais, M.M.L. Ribeiro Carrott, J.A. Menéndez, *Micropor. Mesopor. Mater.* **47**, 243 (2001).
- [19] Tavagnacco, et al. (2011) *J Phys Chem B* **115**, 10957 (2011).
- [20] W. L. Jorgensen, D. S. Maxwell, J. Tirado-Rives, *J. Am. Chem. Soc.* **118**, 11225 (1996).
- [21] P. Ungerer, C. Nieto-Draghi, B. Rousseau, G. Ahunbay, V. Lachet, *Journal of Molecular Liquids* **134**, 71 (2007).
- [22] H.J.C. Berendsen, J.P.M. Postma, W.F. van Gunsteren, and J. Hermans, In *Intermolecular Forces*, edited by B. Pullman (Reidel, Dordrecht, 1981), p. 331.
- [23] H.J.C. Berendsen, J.R. Grigera, T.P. Straatsma, *J. Phys. Chem.* **91**, 6269 (1987).
- [24] W.L. Jorgensen, J. Chandrasekhar, J.D. Madura, R.W. Impey, M.L. Klein, *J. Chem. Phys.* **79**, 926 (1983).

- [25] J. L. F. Abascal, and C. Vega, *J. Chem. Phys.* **123**, 234505 (2005).
- [26] C. Herdes, C. Prosenjak, S. Román, E.A. Müller, *Langmuir* **29**, 6849 (2013).
- [27] W.A. Steele, *Surf. Sci.* **36**, 317 (1973).
- [28] H.J.C. Berendsen, D. van der Spoel, R. van Drunen, *Comp. Phys. Comm.* **91**, 43 (1995).
- [29] C. Herdes, T.S. Totton, E.A. Müller, *Fluid Phase Equilibria* **406**, 91 (2015).
- [30] C. Herdes, C. Petit, A. Mejía, E.A. Müller, *Energy Fuels*, *in press* DOI: [10.1021/acs.energyfuels.8b00200](https://doi.org/10.1021/acs.energyfuels.8b00200), (2018)
- [31] C.H. Bennett, *J. Compu. Phys.* **22**, 245 (1976).
- [32] R. Olsen, B. Kvamme, T. Kuznetsova, *Fluid Phase Equilibria* **418**, 152 (2016).
- [33] S. Brunauer, L.S. Deming, W.E. Deming, E. Teller. *J. Am. Chem. Soc.* **62**, 1723 (1940).
- [34] M. Sevilla, A.B. Fuertes. *Carbon* **47(9)** (2009) 2281.
- [35] J.C.D. Brand, G. Eglinton, *Applications of spectroscopy to organic chemistry*. (Oldbourne Press, London, 1965) p. 110.
- [36] X. Liu, C. Giordano, M. Antonietti. *Small* **10**, 193 (2014).
- [37] C. Moreno-Castilla, M.V. López-Ramón, F. Carrasco-Marín, *Carbon* **38(14)** 1995 (2000).
- [38] D. Leaist, L. Hui, *J. Phys. Chem.* **94**, 8741 (1990).
- [39] W.E. Price, *J. Chem. Soc., Faraday Trans. 1* **85**, 415 (1989).
- [40] J.R. Robalo, S. Huhmann, B. Kokschi, A. Vila-Verde, *Chem*, **3**, 881-897 (2017).
- [41] M.T. Geaballe, A.G. Skillman, A. Nicholls, J.P. Guthrie, P.J. Taylor, *J. Comput. Aided Mol. Des.* **24**, 259 (2010).

List of figure captions:

- Figure 1.** Schematic representation of the different procedures followed to obtain the pistachio shell-derived HCs.
- Figure 2.** A graphical description of the BAR method. Identical MD simulations cells differ only on the values of λ (intensity) screening the energetic contribution of a solute immerse in a water bath and span from pure water ($\lambda=0$) to the diluted CAF/water system ($\lambda=1$).
- Figure 3.** N₂ adsorption isotherms at 77 K for non-pyrolyzed and pirolyzed HCs.
- Figure 4.** SEM micrographs of samples HC and HC_Pir.
- Figure 5.** SEM micrographs of samples HC_Ba and HC_Ba_Pir.
- Figure 6.** SEM micrographs of samples HC_Ac and HC_Pir_Ac.
- Figure 7.** FT-IR spectra of the HCs.
- Figure 8.** Experimental caffeine adsorption isotherms onto selected HCs.
- Figure 9.** Combined bulk-pore simulation cell for CAF self-diffusion studies. With a bare 2 nm slit-like carbon pore, the length of the simulation cell is 20 nm with 10 nm in depth.
- Figure 10.** Extrapolated experimental and calculated MD CAF self-diffusion comparison with all studied water models.
- Figure 11.** a) The energetic evolution of the studied CAF/Water/2 nm HC system and b) Selected snapshots relative to the time of the energetic evolution.
- Figure 12.** a) Steps needed to determine the free energy of solvation (ΔG) via BAR system and b) contribution to the CAF ΔG of solvation from consecutives 21 λ -points.

Figure 1)


	HTC	Pyrolysis, N₂
Pistachio Shell (PS) 	No chemicals added → HC HNO ₃ → HC_Ac KOH → HC_Ba	HC_Pyr HC_Ac_Pyr HC_Ba_Pyr

Figure 2)

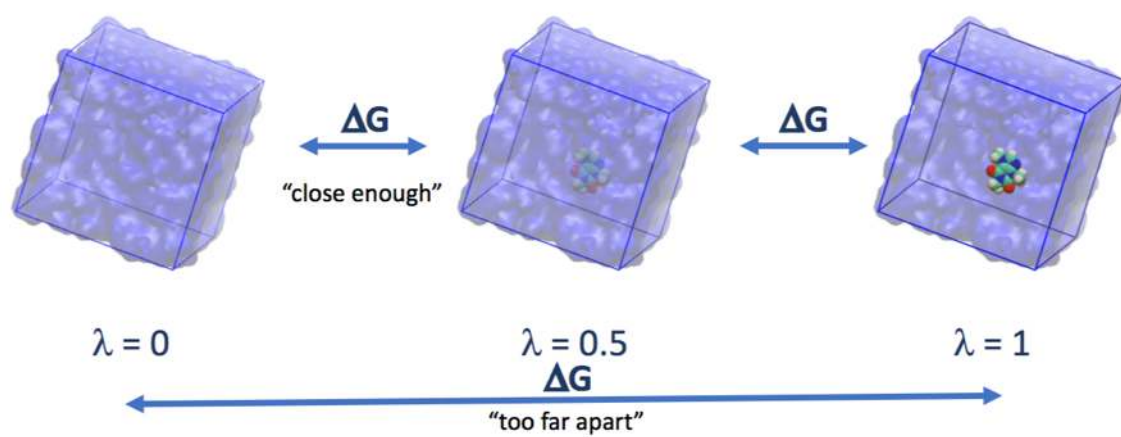


Figure 3)

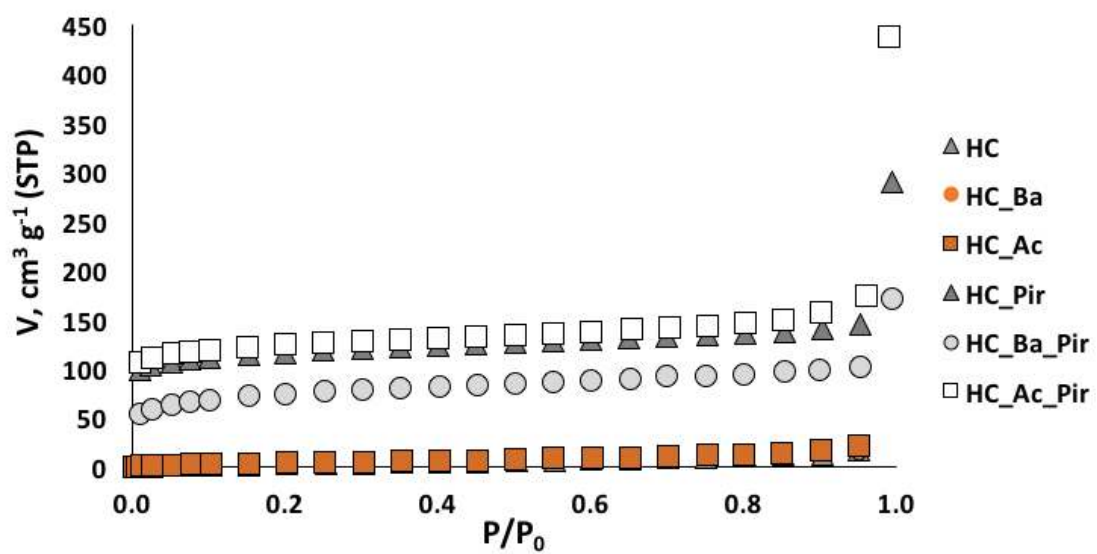


Figure 4)

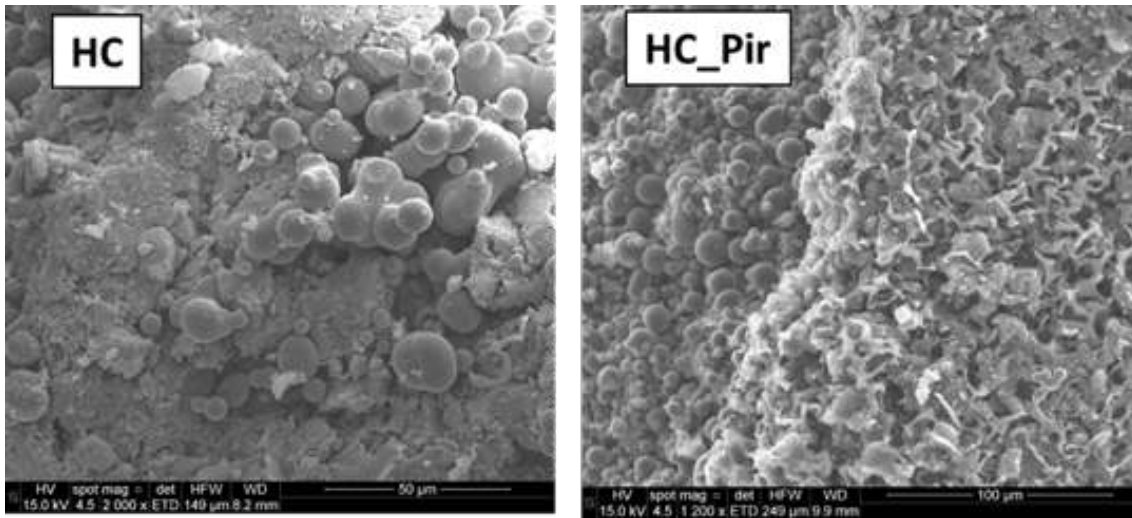


Figure 5)

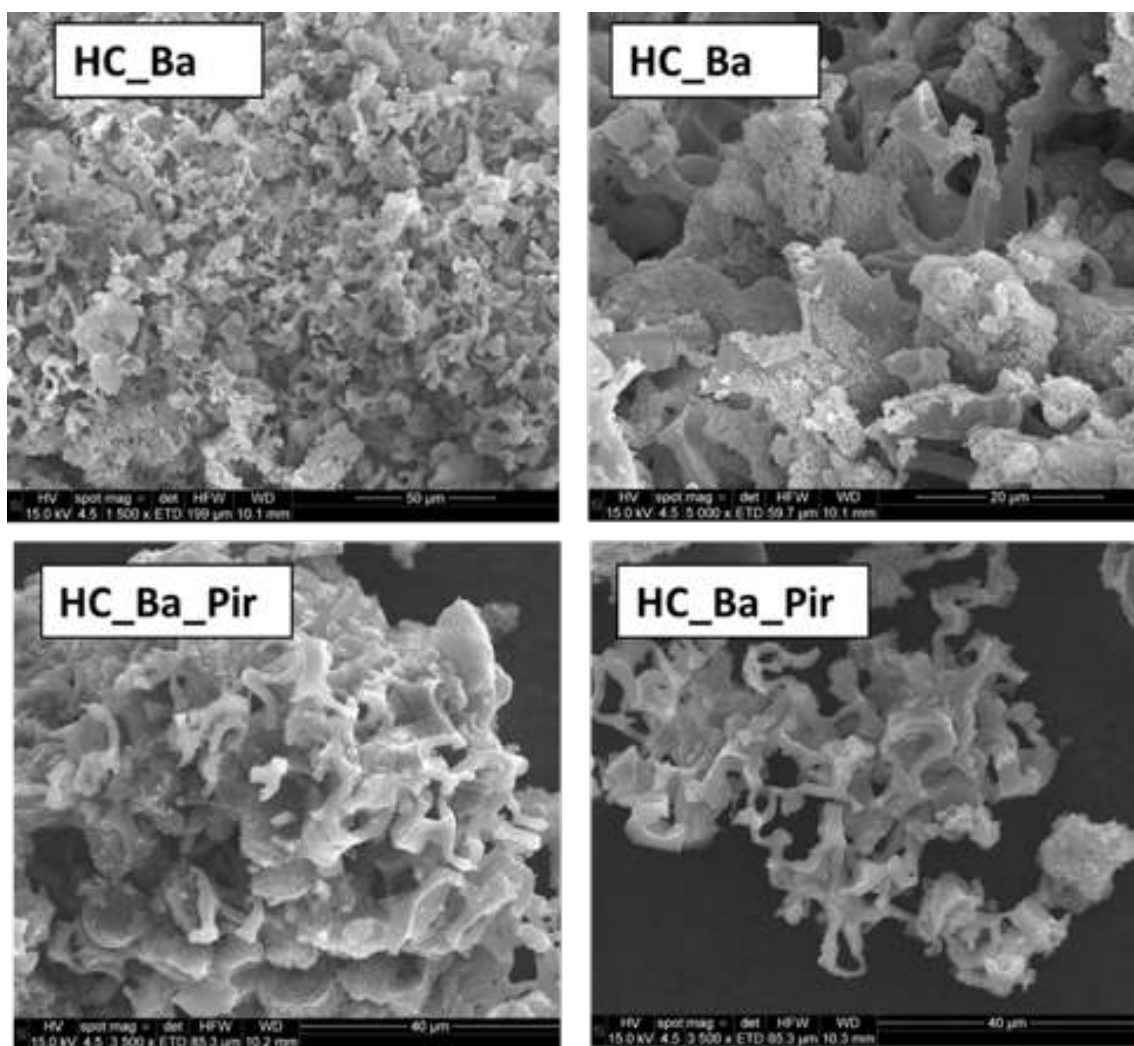


Figure 6)

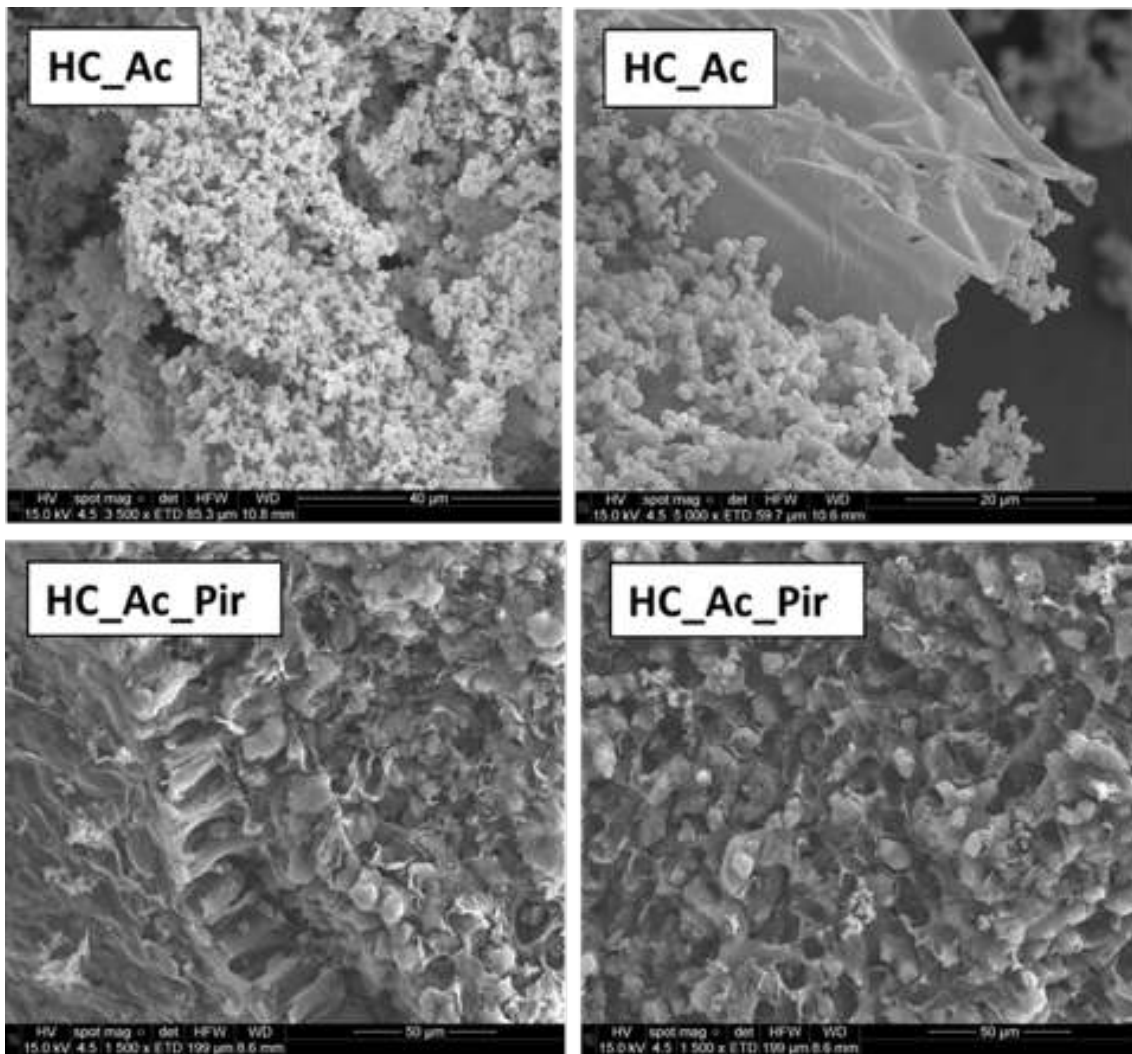


Figure 7)

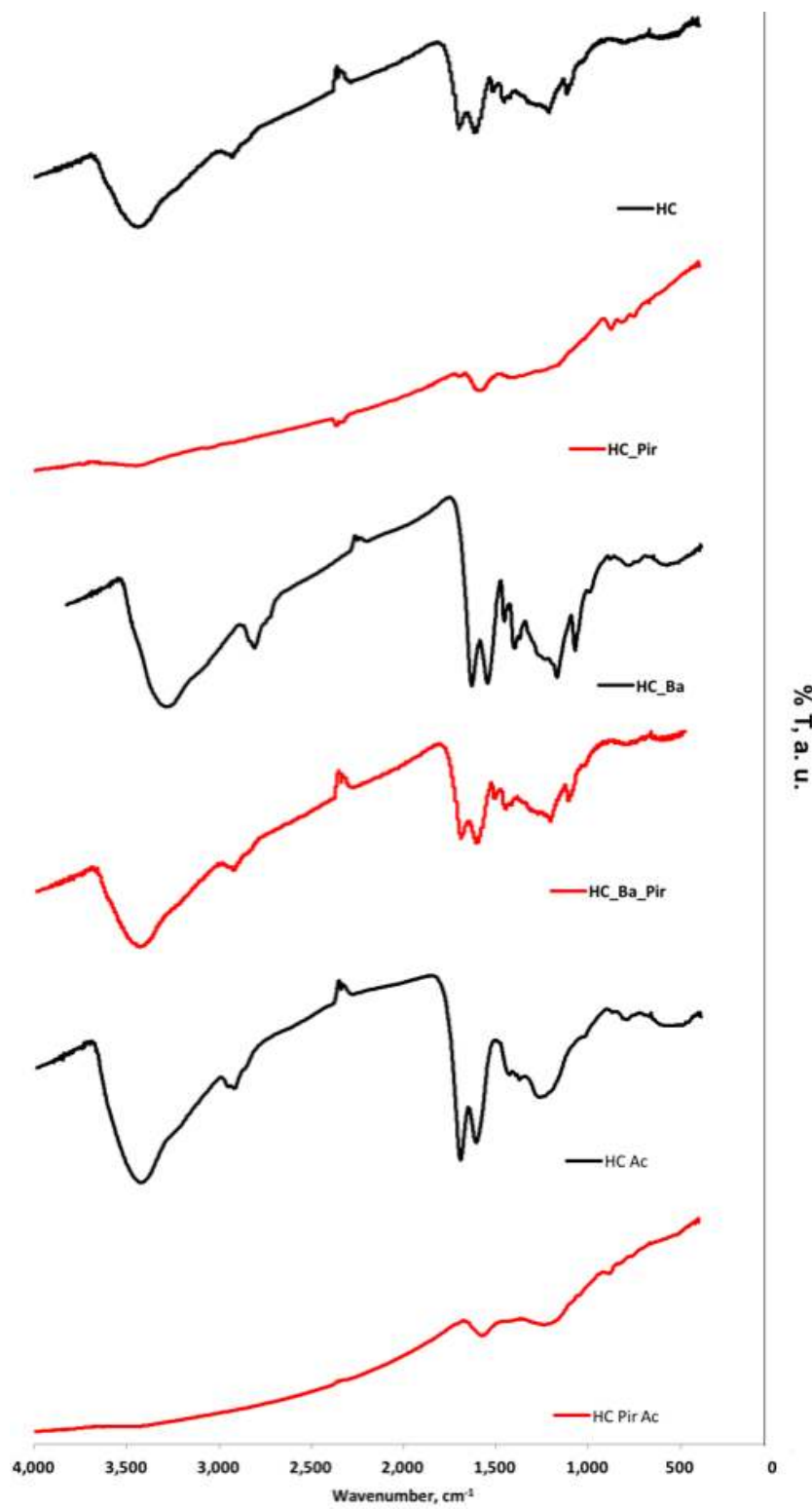


Figure 8)

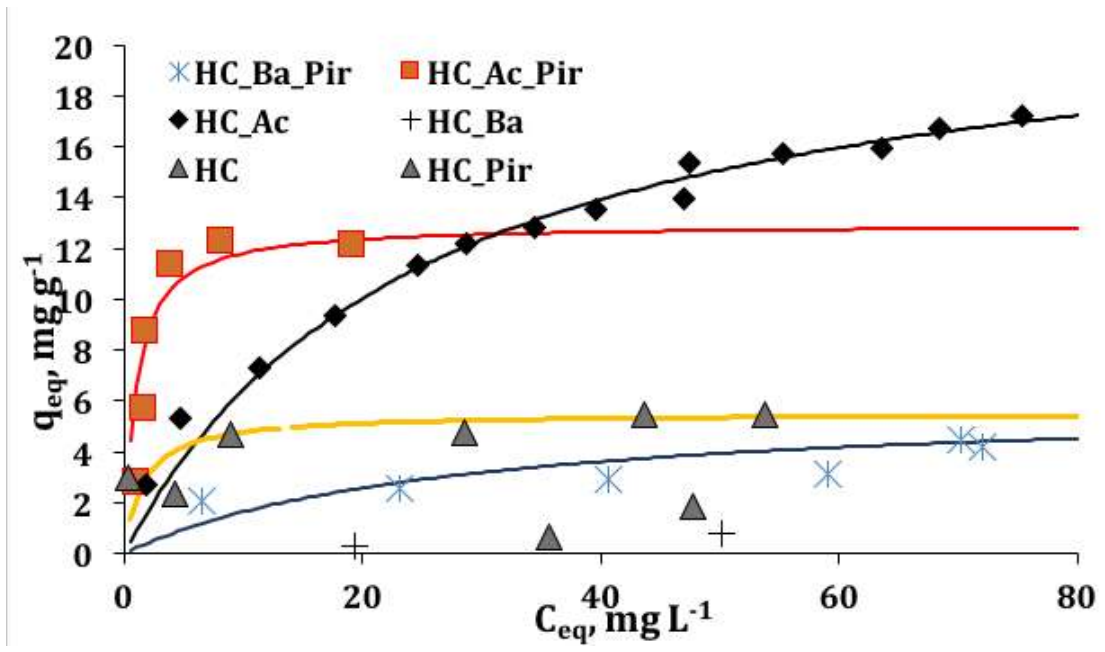


Figure 9)

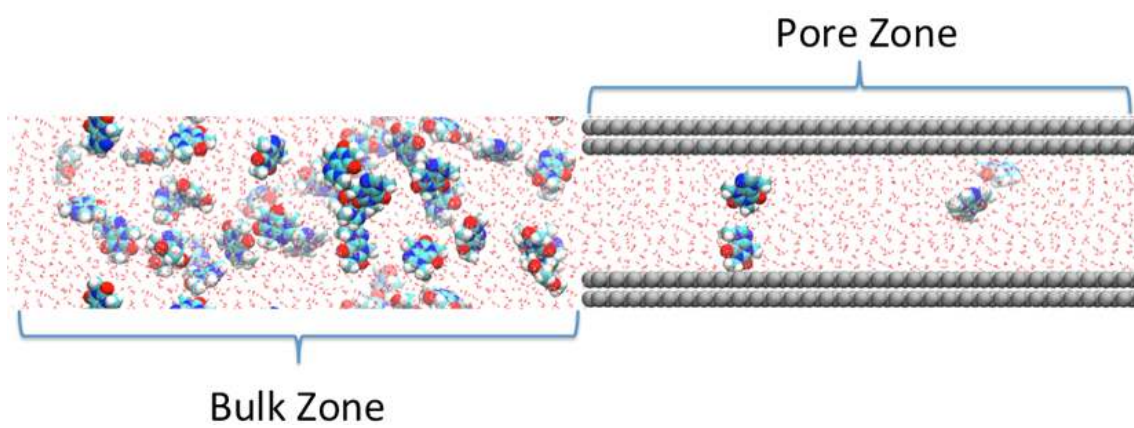


Figure 10)

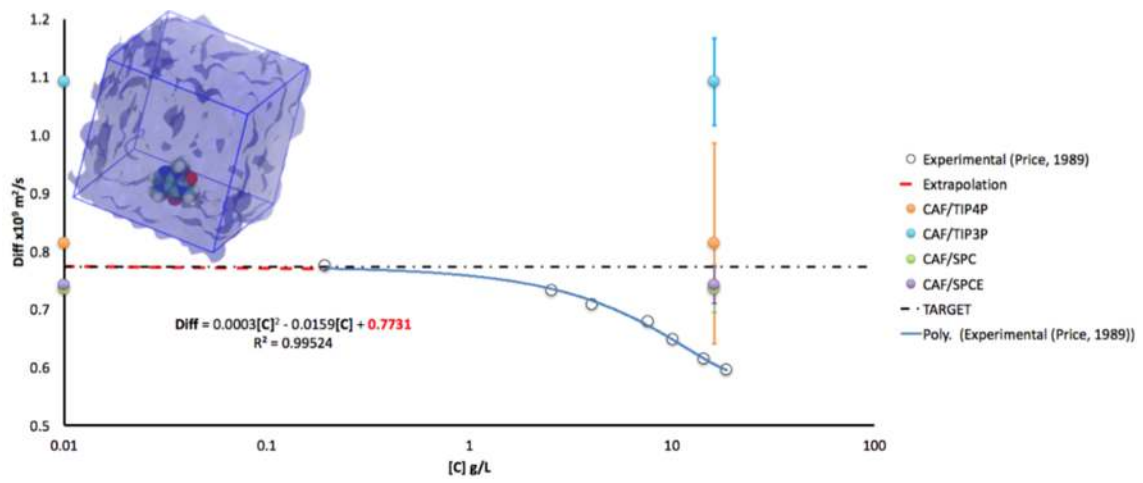


Figure 11)

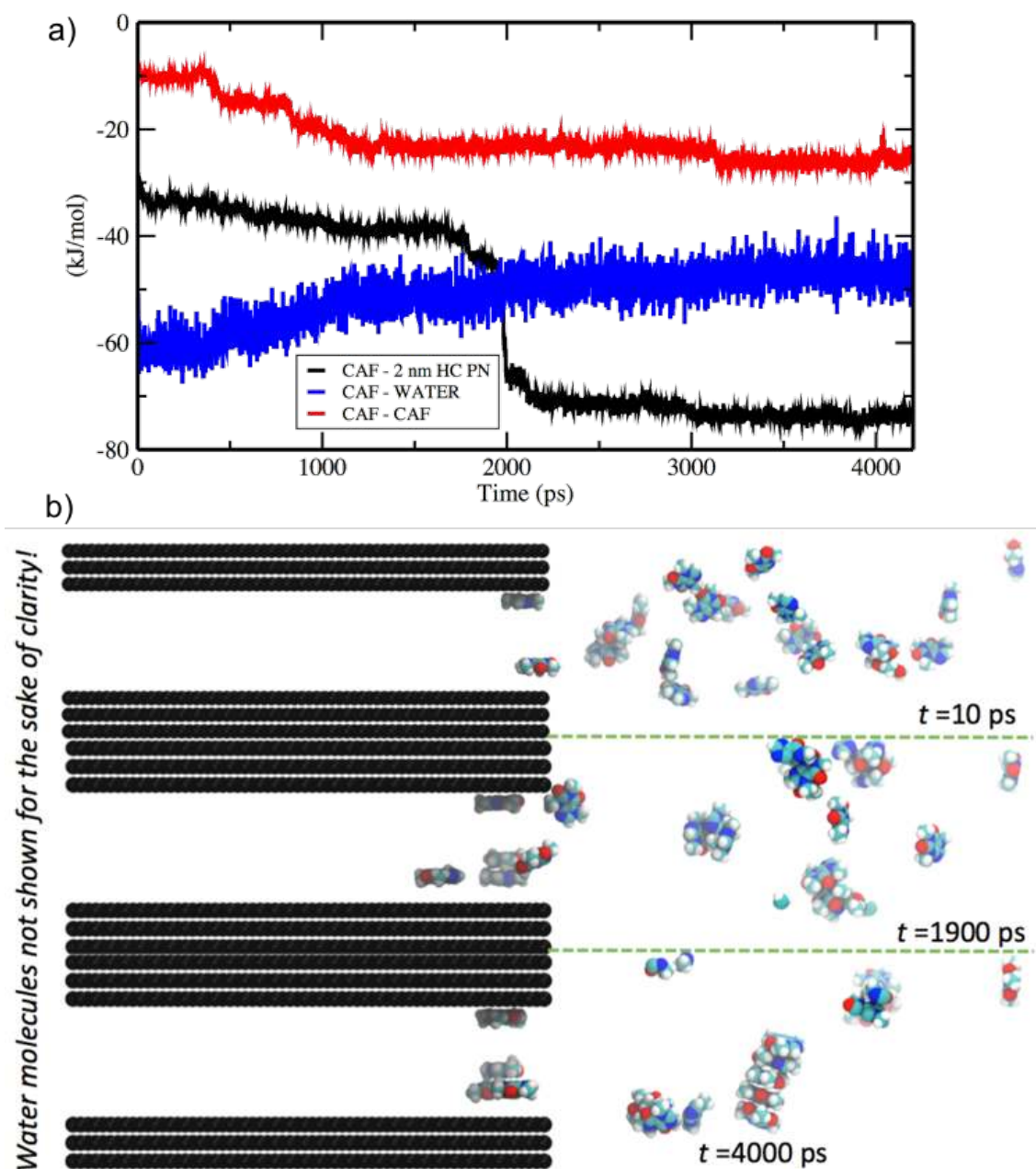


Figure 12)

